Solid State Ionics 141-142 (2001) 243 - 252

Formation of Bronzes during Temperature-programmed Reduction of MoO_3 with Hydrogen - An In situ XRD and XAFS Study

T. Ressler*, J. Wienold, R.E. Jentoft

Department of Inorganic Chemistry, Fritz-Haber-Institute of the MPG, Faradayweg 4-6, 14195 Berlin, Germany

* Corresponding author: e-mail ressler@fhi-berlin.mpg.de, phone +49 30 8413 3192, fax +49 30 8413 4401

Submitted 15 August 2000; accepted 26 November 2000

Abstract

The temperature-programmed reduction of MoO_3 from 300 K to 773 K in 50 vol-% hydrogen in He (10^5 Pa) at different heating rates (0.1, 0.2, and 5 K/min) was investigated by in situ XRD and XAFS. At heating rates of ~ 0.1 and ~ 0.2 K/min the formation of the molybdenum bronze $H_{0.34}MoO_3$ was observed by in situ XRD in the early stage of the reduction of MoO_3. At a heating rate of 5 K/min the formation of a more disordered bronze (H_xMoO_3 with x ~ 0.07) prior to the detection of the product phase MoO_2 was observed by in situ XAFS. In both studies the consumption of the bronze was found prior to the complete reduction of MoO_3. A simplified mechanism for the temperature-programmed reduction of MoO_3 in hydrogen is proposed that includes (i) incorporation of H_2 in the MoO_3 bulk and formation of a more or less ordered bronze, (ii) consumption of the bronze and formation of nucleation site for MoO_2, (iii) nucleation of MoO_2 and nuclei growth.

Keywords: molybdenum oxide, TPR, reduction, bronze, in situ, XRD, XAFS

Introduction

Molybdenum oxide based systems are highly active heterogeneous catalysts for the selective oxidation of hydrocarbons [1, 2]. Because the catalytically active phase appears to be neither MoO_3 nor MoO_2 but rather a partially reduced molybdenum oxide, the reduction of MoO_3 or molybdenum mixed oxides with hydrogen or light alkenes has been investigated in great detail in the past [3, 4]. Recently, we reported the formation of the molybdenum suboxide Mo_4O_{11} from a parallel reaction of MoO_3 and MoO_2 during reduction of MoO_3 with hydrogen [5]. However, no crystalline intermediate phase was detected and the reduction of MoO_3 to MoO_2 was concluded to be a one step process. Nucleation-growth kinetics were found to govern the reduction of MoO_3 with hydrogen over a large range of reaction temperatures and H_2 partial pressures. Interestingly, the apparent activation energy of the reduction of MoO_3 with hydrogen was found to decrease with increasing hydrogen concentrations with no apparent change in the rate-determining step.

However, despite the number of studies on phase evolution and kinetics of the reduction of MoO_3 to MoO_2 much less is known about the early stage of the reduction of MoO_3 prior to the formation of crystalline products. Thöni and Hirsch [6] and Gai [7] proposed that oxygen vacancies originating in the course of reduction resulted in the formation of shear-planes in molybdenum trioxide. In order to further elucidate the early stage of the reduction of MoO_3 with hydrogen, in particular structural changes in MoO_3 or the evolution of phases prior to the formation of MoO_2, we have performed in situ XRD and XAFS studies on the temperature-programmed reduction of MoO_3. The potentials of in situ X-ray absorption spectroscopy for structural studies especially in conjunction with in situ X-ray diffraction have been described in a recent publication [5]. In this work the two complementary techniques were employed to elucidate both phase compositions and detailed structural changes in the phases present under reaction conditions. Therefore, both the near-edge structure and the extended fine structure of Mo K edge spectra are analyzed in detail. The former can yield quantitative phase composition and the average Mo valence, the latter affords the evolution of the local structure of the nearest neighbor shells around the Mo absorber. Here, a new approach to the analysis of XAFS data of phase mix-

tures, particularly important for in situ studies in solid state chemistry is presented.

Experimental

MoO_3 preparation

Molybdenum trioxide (MoO_3) was prepared by thermal decomposition of ammonium heptamolybdate (AHM), $(NH_4)_6Mo_7O_{24}?4H_2O$ (*Aldrich Co.*), in flowing synthetic air (RT – 773 K, 2 K/min) [5]. Specific areas were calculated by applying the BET method to the nitrogen adsorption isotherms obtained at liquid nitrogen temperature on samples outgassed at 473 K using a *Quantachrom* adsorption instrument. A BET surface area of ~ 5 m^2/g was determined for MoO_3 prepared from AHM. Peak profile analysis of XRD patterns yields an average crystallite size of ~ 75 nm.

X-ray diffraction

In situ XRD experiments were carried out in *Bragg Brentano* scattering geometry on a *STOE STADIP P* diffractometer equipped with a secondary monochromator (Cu $K_?$ radiation) and a scintillation counter operated in a stepping mode. The in situ cell consisted of a *Bühler HDK S1* high temperature diffraction chamber. Typically, 15 mg of sample are uniformly spread on the heating band. The gas phase composition was analyzed by mass spectrometry. XRD measurements reported here were conducted under atmospheric pressure in flowing reactants (~ 100 ml/min total flow). The in situ XRD set-up used is described in more detail in [5]. Calculation of theoretical X-ray powder patterns and lattice constant refinements were done using the software PowderCell v2.1 [8].

In situ X-ray Absorption Spectroscopy

For in situ XAFS experiments molybdenum oxide was mixed with boron nitride (ratio 1:3) and 30 mg of the mixture was pressed with a force of 1 ton into a 5 mm in diameter self-supporting pellet. The absorption jump, ??x, at the Mo K edge was ~ 1.5. In situ XAS experiments were carried out in a flow-reactor at atmospheric pressure. Temperature programmed reduction experiments were conducted in flowing reactants (40 ml/min) at a constant heating rate of 5 K/min. The composition of the gas phase was continuously monitored using a mass spectrometer (QMS200 from *Pfeiffer*). The in situ XAFS set-up used is described in more detail in [5]. In situ XAS experiments were performed at the Mo K edge (19.999 keV) at beamline X1.1 at the *Hamburger Synchrotron Radiation Laboratory*, HASYLAB, using a Si(311) double crystal monochromator. The storage ring operated at 3.6 GeV with injection currents of 150 mA.

X-ray absorption fine structure (XAFS) analysis was performed using the software package WinXAS v2.0 [9] following recommended procedures from the literature [10]. Background subtraction and normalization were performed by fitting linear polynomials to the pre-edge and the post-edge region of an absorption spectrum, respectively. The Mo K edge absorption threshold was determined from the first root in the first derivative of the near-edge region (XANES) (in the following edge shifts are reported relative to the first inflection point in the Mo metal K edge XANES at 19999 eV). Reduction or oxidation of Mo causes a shift in the Mo K absorption edge to lower or higher photon energies, respectively, and, hence, the edge shift can be used to identify changes in Mo valence during reaction.

Principal component analysis (PCA) of the Mo K edge XANES was used to identify Mo oxide phases present during the reduction of MoO_3. Given a library of molybdenum reference spectra, PCA can identify number and type of phases present in a set of experimental XANES spectra. Subsequently, a least-squares fitting procedure is applied to obtain the evolution of the amount of each reference phase during the reaction. Hence, XANES analysis can afford information on low concentration or amorphous phases not readily available with XRD. More details on PCA analysis of XAFS spectra can be found in Ref. [11].

For the absorption fine structure (EXAFS) analysis, a smooth atomic background, $?_0(k)$, was obtained using cubic splines. The radial distribution function FT(?(k)) was obtained by Fourier transforming the k^3-weighted experimental ?(k) function, multiplied by a Bessel window, into the R space. EXAFS data analysis was carried out using theoretical backscattering phases and amplitudes calculated with the ab-initio multiple-scattering code FEFF7 [12]. Single scattering and multiple scattering paths in the employed model structures were calculated up to 5.0 Å with a lower limit of 2.0 % in amplitude with respect to the strongest backscattering path. EXAFS fitting and simulation were performed using the standard EXAFS formula (k range from 3.5 to 15 $Å^{-1}$, R range 0.9 to 4.4 Å). For mixtures of MoO_2 and MoO_3 the ratio of the two corresponding theoretical XAFS functions was set to the ratio of MoO_2 and MoO_3 as determined by the XANES analysis. Structural parameters that are determined by a least-squares EXAFS fit to experimental spectra are (i) one E_0 shift for all paths in the MoO_3 structure and one E_0 shift for those in the MoO_2 structure, (ii) one Debye temperature for oxygen backscatterer, and one for molybdenum in MoO_2 and one for molybdenum in MoO_3, (iii) selected Mo-O and Mo-Mo coordination shell distances (Table 1), (iv) third cumulants for MoO_2 and MoO_3. Coordination numbers (CN) were kept invariable in the refinement. These restrictions were necessary to reduce the number of free running parameter (N_{free}) to less than the number of independent parameters (N_{ind}) in the experimental data used. EXAFS refinements reported here were carried out in R space to magnitude and imaginary part of a Fourier transformed k^3-weighted experimental ?(k). More details about the XAFS fitting procedure employed can be found in reference [13].

Results

Figure 1a and b depict XRD patterns measured in situ during temperature programmed reduction of MoO_3 in 50 vol-% H_2 (in He) with an effective heating rate of 0.2 K/min and 0.12

K/min, respectively. At a heating rate of 0.2 K/min the formation of MoO_2 can be seen at ~ 613 K. In addition, diffraction peaks that can not be assigned to MoO_3 or MoO_2 were observed at this temperature (* in Figure 1a). Upon further heating these additional peaks disappear and all peaks present can be assigned to either MoO_3 or MoO_2 (Figure 2). Eventually, at 773 K the TPR results in the formation of molybdenum metal (? in Figure 1a). At a heating rate of 0.12 K/min additional diffraction peaks that do not belong to MoO_3 or MoO_2 were also observed (* in Figure 1b), even more pronounced than in Figure 1a, and prior to the formation of detectable amounts of MoO_2 at 603 K. From a comparison with known references (Figure 2) the additional diffraction peaks observed (* in Figure 2 (D)) were assigned to the molybdenum bronze $H_{0.34}MoO_3$ [14]. Nearest neighbor shell distances and lattice constants for MoO_3 and $H_{0.34}MoO_3$ at elevated temperature are given in Table 1. A structural model of $H_{0.34}MoO_3$ is depicted in Figure 3. In this bronze the orthorhombic layer structure of MoO_3 is retained and hydrogen is located in the layers at oxygen atoms of corner-sharing MoO_6 units along the [100] direction.

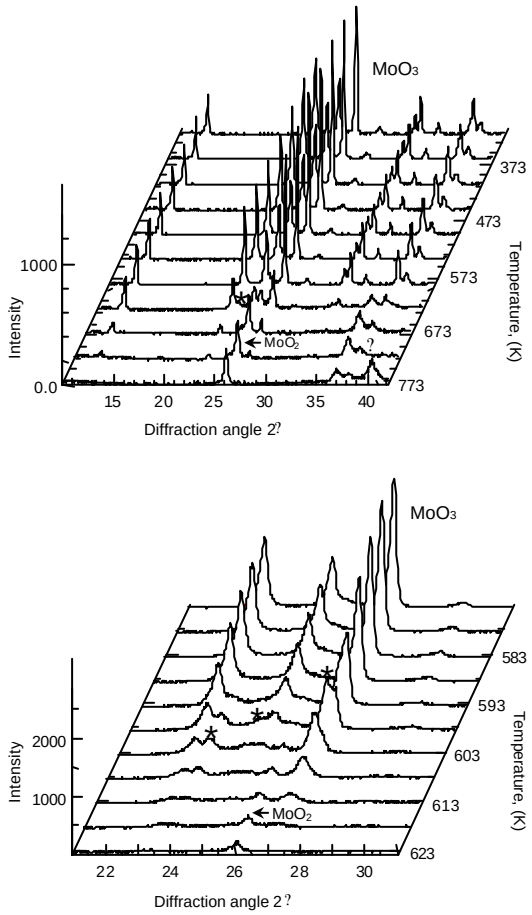

Figure 1: Evolution of XRD patterns measured during TPR of MoO_3 in 50 vol-% H_2 (in He) at (a) 0.2 K/min and (b) 0.12 K/min. Peaks indicated with an * correspond to $H_{0.34}MoO_3$. ? denotes molybdenum metal.

In Figure 4 the evolution of Mo K edge XANES spectra measured during TPR of MoO_3 in 50 vol-% H_2 (5 K/min) is depicted. At ~ 673 K a transition from the distinct near-edge structure of MoO_3 to that of MoO_2 can be seen. Principal component analysis of the spectra in Figure 4 revealed two major phases (MoO_3 and MoO_2) to be sufficient to reconstruct the experimental data. A refinement of the sum of MoO_3 and MoO_2 reference spectra to the experimental spectra afforded the quantitative evolution of the two phases during TPR of MoO_3 as shown in Figure 5. In addition, the shift in photon energy of the Mo K edge during TPR was determined (Figure 5). Already prior to the formation of detectable amounts of MoO_2 at temperatures between 473 K and 673 K a slight shift of the Mo K edge towards lower photon energies can be observed. This indicates a reduction of molybdenum in this region that is not accompanied by the formation of an additional phase, which is sufficiently ordered for detection.

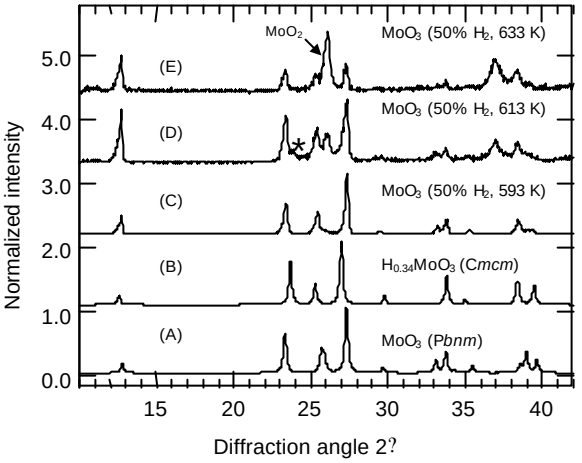

Figure 2: Comparison of theoretical powder patterns (A and B) of orthorhombic MoO_3 (*Pbnm*, {5-508}) and $H_{0.34}MoO_3$ (*Cmcm* , {34-1230} [14]), and XRD patterns measured in situ during TPR of MoO_3 (Figure 1a). (C) MoO_3 at 593 K, (D) mixture of MoO_3, $H_{0.34}MoO_3$ (denoted by *), and MoO_2 at 613 K, (E) mixture of MoO_3 and MoO_2 at 633 K.

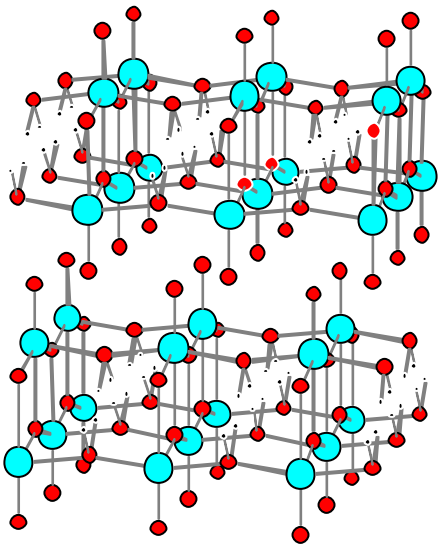

Figure 3 Structural model of orthorhombic $H_{0.34}MoO_3$ (*Cmcm* [14]) (*small circles*: hydrogen, *medium circles*: oxygen, *large circles*: molybdenum). Orthorhombic MoO_3 possesses a very similar layer structure without the hydrogen atoms.

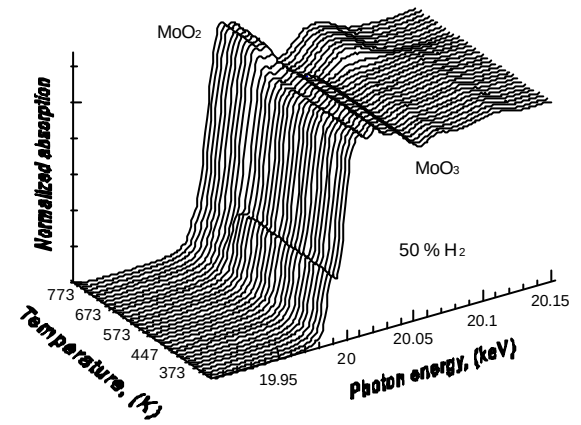

Figure 4: Evolution of Mo K edge XANES during TPR of MoO_3 in 50 vol-% hydrogen at a heating rate of 5 K/min. Initial and product phase are indicated.

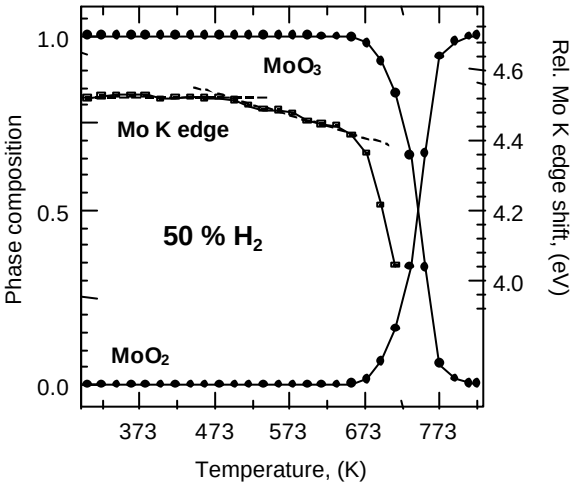

Figure 5: Evolution of phase composition during TPR of MoO_3 in 50 vol-% H_2 (Figure 4) together with the relative Mo K edge shift (not shown above 713 K to emphasize low temperature part). Dashed lines indicate a change in slope of the edge-shift curve at 473 K corresponding to a slight reduction of the molybdenum oxide between 473 K and 673 K.

The evolution of the Fourier transformed EXAFS ?(k) obtained from the spectra in Figure 4 is shown in Figure 6. At a temperature of 673 K a transition from the FT(?(k)) of MoO_3 to that of MoO_2 can be seen. The considerable reduction in amplitude of the Mo-Mo shells in Figure 6 is mainly caused by the increasing temperature. However, the evident change in the shape of the "Mo-O" peaks in Figure 6 can not solely be ascribed to a temperature effect and, thus, indicates a change in the short-range order around the Mo absorber at temperatures between 473 K and 673 K. To further elucidate this change in the short-range order of MoO_3 during TPR with hydrogen, a refinement of theoretical EXAFS functions to the experimental spectra was performed. As an example, Figure 7 shows the fit of a sum of the EXAFS functions of MoO_3 and MoO_2 to the experimental FT(?(k)) of a mixture of MoO_3 and MoO_2 at 733 K. The structural parameters refined are given in Table 2. The most prominent single and multiple scattering paths present in the two structures are depicted in Figure 7 underlining the complexity of the system studied. However, by employing constraints on the refinement as described above, reliable information about the structural changes that MoO_3 undergoes during TPR can be obtained. Moreover, in the work presented here, the relative evolution of the nearest neighbor distances around the Mo absorber is more important than their absolute values to interpret the structural modification observed in terms of a reaction mechanism.

Table 1. Nearest neighbor shell distances in MoO_3 at different temperatures and in $H_{0.34}MoO_3$ at 593 K. Distances were calculated after a refinement of the lattice constants [8] of the orthorhombic MoO_3 (*P*bnm, {5-508}) and $H_{0.34}MoO_3$ (*C*mcm, {34-1230} [14] a=3.895 Å, b=14.070 Å, c=3.737 Å) structure to experimental X-ray powder patterns measured in situ at temperature (MoO_3 (300 K) a = 3.964 Å, b = 13.880 Å, c = 3.697 Å; MoO_3 (593 K) a = 3.978 Å, b = 14.082 Å, c = 3.699 Å; MoO_3 (748 K) a = 3.992 Å, b = 14.237 Å, c = 3.701 Å; $H_{0.34}MoO_3$ (593 K) a = 3.882 Å, b = 14.301 Å, c = 3.724 Å). Shells that exhibit the most prominent differences between the MoO_3 and the $H_{0.34}MoO_3$ structure are highlighted.

Shell	MoO_3 300 K, (Å)	MoO_3 593 K, (Å)	MoO_3 748 K, (Å)	$H_{0.34}MoO_3$ 593 K, (Å)
Mo - O	1.671	1.698	1.716	1.696
Mo - O	1.735	1.742	1.748	1.938
Mo - O	1.948	1.952	1.954	1.938
Mo - O	1.948	1.952	1.954	1.959
Mo - O	2.251	2.260	2.268	1.959
Mo - O	2.332	2.370	2.395	2.459
Mo - Mo	3.438	3.477	3.504	3.529
Mo - Mo	3.696	3.699	3.701	3.724
Mo - Mo	3.963	3.978	3.992	3.882

Table 2. Structural parameters of a mixture of MoO_3 and MoO_2 at 733 K in 50 % H_2 (Figure 7) obtained from a refinement of a sum of theoretical EXAFS functions calculated for an orthorhombic MoO_3 structure and a monoclinic MoO_2 structure (k = 3.0 to 15.3 $Å^{-1}$, R = 0.7 to 4.2 Å, N_{ind} = 29, N_{free} = 19, 16 single scattering paths and 20 multiple scattering paths). Parameters refined are (i) for MoO_3, ?(O) = 1360 K, ?(Mo) = 376 K, E_0 (MoO_3) = -1.9, (ii) for MoO_2, ?(O) = 520 K, ?(Mo) = 373 K, E_0 (MoO_2) = -3.4 (?: Debye temperature). The fit residual amounted to 4.6.

	MoO_3			MoO_2		
Shell	CN	R, (Å)	$?^2$, ($Å^2$)	CN	R, (Å)	$?^2$, ($Å^2$)
Mo-O	1 [f]	1.693 [c]	0.0024 [c]	2 [f]	1.925 [c]	0.0145 [c]
Mo-O	1 [f]	1.725	0.0023 [c]	2 [f]	1.931 [c]	0.0146 [c]
Mo-O	2 [f]	1.982 [c]	0.0026 [c]	2 [f]	2.005 [c]	0.0149 [c]
Mo-O	1 [f]	2.275	0.0028 [c]			
Mo-O	1 [f]	2.401	0.0028 [c]			
Mo-Mo	2 [f]	3.421	0.0087 [c]	1 [f]	2.544	0.0079 [c]
Mo-Mo	2 [f]	3.696	0.0088 [c]	1 [f]	3.204	0.0087 [c]
Mo-Mo	2 [f]	3.921	0.0088 [c]	4 [f]	3.704 [c]	0.0088 [c]
Mo-Mo				2 [f]	3.740 [c]	0.0088 [c]
Mo-Mo				2 [f]	3.802 [c]	0.0088 [c]

[f] indicates parameters that were fixed in the refinement, [c] denotes parameters that were correlated to other parameters in the fit.

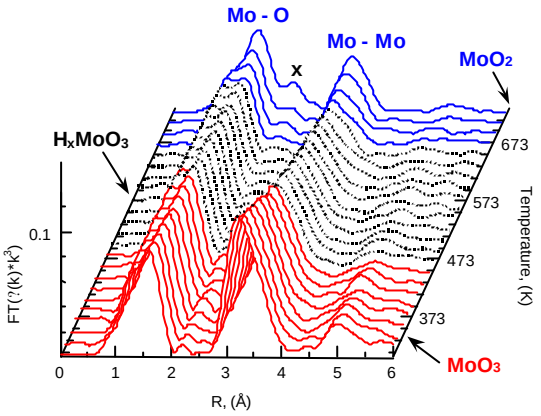

Figure 6: Evolution of Mo K edge FT(?(k)) during TPR of MoO_3 in 50 vol-% H_2 (Figure 4). The first peak (~ 1.5 Å) corresponds to Mo-O backscatterer, the second peak at ~ 3.5 Å corresponds to Mo-Mo backscatterer. (x) denotes the formation of edge-sharing octahedra in the distorted rutile structure of MoO_2. Three regions are indicated (i) MoO_3, initial material, (ii) $H_{0.34}MoO_3$, mixture of MoO_3 and $H_{0.34}MoO_3$, (iii) MoO_2, mixture of MoO_2 and MoO_3.

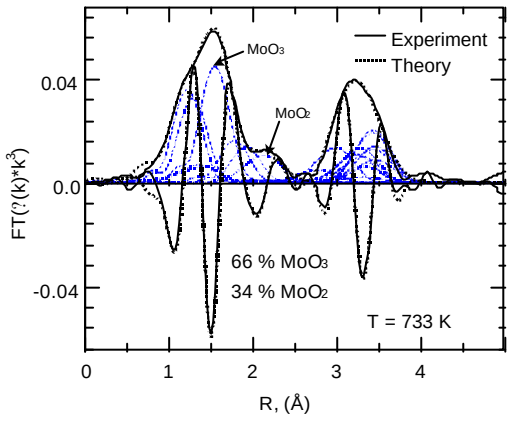

Figure 7: Refinement of a sum of theoretical EXAFS functions of MoO_3 and MoO_2 to an experimental FT(?(k)) at 733 K in 50 vol-% H_2 (Figure 6). The phase composition was obtained from a XANES analysis. Thin dashed lines correspond to prominent single back-scattering paths in the MoO_3 structure, thin dotted lines to those in the MoO_2 structure. Structural parameters obtained from the fit are given in Table 2.

Figure 8 shows the evolution of selected Mo-O and Mo-Mo distances in the MoO_3 structure during TPR in 50 vol-% H_2 (Figure 6). In the temperature region from 473 K and 673 K significant deviations from the expected linear thermal expansion of MoO_3 can be noticed. Interestingly, prior to the detection of MoO_2 at 673 K, the Mo-O and Mo-Mo distances return to the values expected for MoO_3 at this temperature. For comparison, the evolution of selected Mo-O distances in MoO_3 during heat treatment in He is depicted in Figure 9. The different slopes of the three traces in Figure 9 confirms an anisotropic thermal expansion of MoO_3 (increased expansion perpendicular to the layers in Figure 3) that is evident from the structural parameters of MoO_3 at different temperatures given in Table 1. The good agreement of the XRD and XAFS data on the structural evolution of MoO_3 at elevated temperatures confirms the reliability of the EXAFS analysis approach taken in this work.

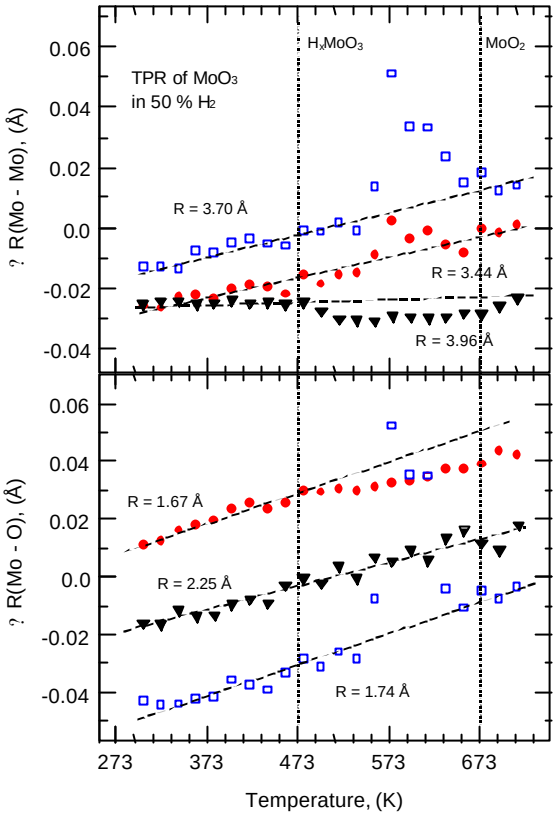

Figure 8: Evolution of Mo-O (bottom) and Mo-Mo (top) distances in MoO_3 (relative to the crystallographic distances *R* in Table 1) during TPR in 50 vol-% H_2. Dashed lines indicate on-set of Mo K edge shift (H_xMoO_3, Figure 5) and on-set of the formation of MoO_2 (Figure 5).

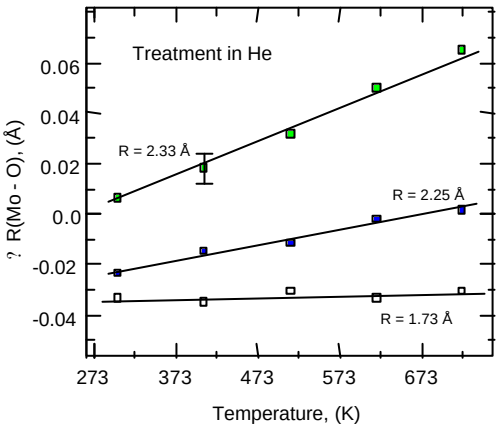

Figure 9: Evolution of Mo-O distances in MoO_3 (relative to the crystallographic distances *R* in Table 1) during temperature treatment in He. The different slopes in the three curves correspond to an anisotropic thermal expansion of MoO_3 with a larger expansion in the *b* direction (perpendicular to the layers in Figure 3) (Table 1).

Discussion

In situ XRD and XAFS studies on the temperature-programmed reduction of MoO_3 were performed to elucidate structural changes in the early stage of the reduction prior to the formation of detectable amounts of MoO_2 (limits ~ 5 % for XRD and ~ 1 % for XAFS). Heating rates of ? 0.2 K/min

resulted in the formation of an additional crystalline phase (in situ XRD, Figure 1) which was identified to be similar to the molybdenum bronze $H_{0.34}MoO_3$ (Figure 2 + 3). Figure 2 indicates that at a heating rate of 0.2 K/min $H_{0.34}MoO_3$ is formed in the early stage of the reduction to MoO_2 and is consumed prior to the complete reduction of MoO_3 to MoO_2. However, under isothermal reduction conditions at temperatures above 623 K or at heating rates of about 2 K/min no crystalline molybdenum bronzes were detected [5].

The in situ XAFS results presented also indicate a slight reduction (Figure 5) and local structural changes in MoO_3 prior to the formation of detectable amounts of MoO_2 (Figure 6 + 8). However, a heating rate of 5 K/min evidently does not permit the formation of sufficiently ordered $H_{0.34}MoO_3$ that could be identified as a third phase in addition to MoO_3 and MoO_2 (Figure 5). Nearest neighbor shell distances for MoO_3 and $H_{0.34}MoO_3$ at 593 K are given in Table 1, with those shells highlighted that exhibit the largest differences in the two otherwise similar structures (Figure 3). It can be seen now from Figure 8 that between 473 K and 573 K the Mo-O shell at R = 1.74 Å (increase) and the Mo-Mo shells at R = 3.70 Å (increase) and at 3.96 Å (decrease) deviate from the expected linear increase with temperature in a way that coincides with the structural differences between MoO_3 and $H_{0.34}MoO_3$ (Table 1). Apparently, also at a heating rate of 5 K/min, hydrogen is incorporated into the MoO_3 bulk prior to the formation of MoO_2. However, the molybdenum bronze formed seems to be rather disordered which can, for instance, be noticed from the Mo-O shell at R = 2.25 Å that does not exhibit the expected decrease while going from MoO_3 to $H_{0.34}MoO_3$. Because the complete reduction of MoO_3 to MoO_2 (valence from +6 to +4) leads to a shift of the Mo K edge of 2.1 eV, an edge shift of ~ 0.07 eV in the early stage of the reduction (Figure 5, T ~ 600 K) indicates an average Mo valence of about +5.93 (assumes a linear relationship between average valence and Mo K edge shift). This would correspond to a bronze with an estimated chemical formula of H_xMoO_3 (with x ~ 0.07) at ~ 600 K in 50 vol-% H_2.

In both the in situ XRD (Figure 2) and the in situ XAFS experiments (Figure 8) it appears, that the bronze formed is consumed at the expense of the formation of MoO_2 prior to the complete reduction of the MoO_3 bulk. In addition, although between 573 K and 673 K the local structure appears to return to that of MoO_3 (Figure 8) no shift of the Mo K edge to higher photon energies is observed. This indicates that the average valence of Mo does not change although the H_xMoO_3 formed seems to be consumed. This can be interpreted such that with increasing reaction temperature the incorporated hydrogen reacts with the MoO_3 bulk and forms "MoO_{3-x}" that eventually serves as nucleation site for the reduction product MoO_2. The structural nature of the "MoO_{3-x}" formed prior to the detection of bulk MoO_2 (for instance, very small MoO_2 nuclei or shear structures) will be the subject of future investigations.

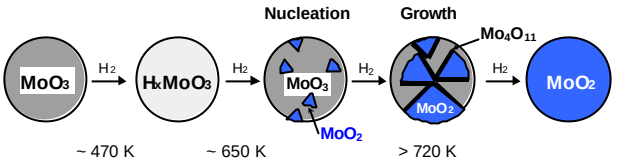

Figure 10: Schematic representation of the reduction of a crystallite of MoO_3 with hydrogen at increasing reaction temperature.

A schematic representation of the mechanism of the temperature-programmed reduction of MoO_3 in hydrogen is given in Figure 10. At a temperature of about 470 K hydrogen is incorporated into the MoO_3 bulk. During this step the orthorhombic layer structure of MoO_3 is retained and appears to be only slightly distorted. With increasing temperature (~ 600 K) the hydrogen in the MoO_3 bulk is consumed and nucleation sites for MoO_2 are being formed. Eventually, at lower hydrogen concentrations (for instance 5 vol-%) the reduction of MoO_3 may be sufficiently delayed to permit the formation of Mo_4O_{11} prior to the complete reduction to MoO_2 [5]. Furthermore, the results presented offer a suitable explanation for the H_2 concentration dependence of the apparent activation energy of the reduction of MoO_3 with hydrogen as reported previously [5]. Evidently, hydrogen is incorporated into the MoO_3 bulk and, hence, can thereby assist in the formation of MoO_2 nuclei. Because the nucleation of MoO_2 is the rate-determining step at this stage of the reduction, an increased concentration of hydrogen in the gas phase and, thus, in the bulk may lead to a decreased apparent activation energy of the reduction process.

Concluding remarks

In this work the temperature-programmed reduction of MoO_3 from 300 K to 773 K in 50 vol-% hydrogen at different heating rates (0.1, 0.2, and 5 K/min) was investigated by in situ XRD and XAFS. At heating rates of 0.1 and 0.2 K/min the formation of the molybdenum bronze $H_{0.34}MoO_3$ was observed by in situ XRD in the early stage of the reduction of MoO_3. At a heating rate of 5 K/min the formation of a more disordered bronze (H_xMoO_3 with x ~ 0.07) prior to the detection of the product phase MoO_2 was observed by in situ XAFS. In both studies the consumption of the bronzes was found prior to the complete reduction of MoO_3. A simplified mechanism for the temperature-programmed reduction of MoO_3 is proposed that includes (i) incorporation of H_2 in the MoO_3 bulk and formation of more or less ordered bronzes, (ii) consumption of the bronze and formation of sites for nucleation of MoO_2, (iii) nucleation of MoO_2 and nuclei growth.

Acknowledgements

We acknowledge the *Hamburger Synchrotron Radiation Laboratory*, HASYLAB, for providing beamtime for this work. TR thanks the *Deutsche Forschungsgemeinschaft*, DFG, for financial support (Habilitationsstipendium). The authors are grateful to Prof. Robert Schlögl for continuous support.

References

[1] R.K. Grasselli, *Catalysis Today* 49 (1999) 141.
[2] J. Haber. E. Lalik, *Catalysis Today* 33 (1997) 119.
[3] P. Arnoldy, J.C.M. de Jonge, J.A. Moulijn, *J. Phys. Chem.* 89 (1985) 4517.
[4] J.R. Regalbuto, J.W. Ha, *Catal. Lett.* 29 (1994) 189.
[5] T. Ressler, R.E. Jentoft, J. Wienold, M.M. Günter, O. Timpe, *J. Phys. Chem. B* 104 (2000) 6360.
[6] W. Thöni, P.B. Hirsch, *Philos. Mag.* 33 (1976) 639.
[7] P.L. Gai, *Philos. Mag.* 43 (1981) 841.
[8] PowderCell v2.1, W. Kraus, G. Nolze, Bundesanstalt für Materialforschung, Berlin (1999).
[9] T. Ressler, *J. Synch. Rad.* 5 (1998) 118.
[10] D.C. Koningsberger, R. Prins, *X-ray Absorption Spectroscopy, Chemical Analysis, 92,* Wiley, New York, 1988.
[11] T. Ressler, J. Wong, J. Roos I.L. Smith, *Environ. Science & Techn.* 34, (2000) 950.
[12] J.J. Rehr, C.H. Booth, F. Bridges, S.I. Zabinsky, *Phys. Rev. B* 49 (1994) 12347.
[13] T. Ressler, S.L. Brock, J. Wong, S.L. Suib, J. Phys. Chem. B 103 (1999) 6407.
[14] P.G. Dickens, J.J. Birtill, C.J. Wright, *J. of Solid State Chem.* 28 (1979) 185.